nature chemical biology

ARTICLES

https://doi.org/10.1038/s41589-019-0336-0

Mycobacterium tuberculosis releases an antacid that remodels phagosomes

Jeffrey Buter[1,12], Tan-Yun Cheng[1,12], Marwan Ghanem[2], Anita E. Grootemaat[3], Sahadevan Raman[1], Xinxin Feng[4], Ashmir R. Plantijn[5], Thomas Ennis[1], Joyce Wang[2], Rachel N. Cotton[1], Emilie Layre[1], Alexandrea K. Ramnarine[1], Jacob A. Mayfield[1], David C. Young[1], Amanda Jezek Martinot[6], Noman Siddiqi[6], Shoko Wakabayashi[6], Helene Botella[7], Roger Calderon[8], Megan Murray[9], Sabine Ehrt[7], Barry B. Snider[10], Michael B. Reed[2], Eric Oldfield[4], Shumin Tan[11], Eric J. Rubin[6], Marcel A. Behr[2], Nicole N. van der Wel[3], Adriaan J. Minnaard[5,12] and D. Branch Moody[1,12]*

***Mycobacterium tuberculosis* (*Mtb*) is the world's most deadly pathogen. Unlike less virulent mycobacteria, *Mtb* produces 1-tuberculosinyladenosine (1-TbAd), an unusual terpene nucleoside of unknown function. In the present study 1-TbAd has been shown to be a naturally evolved phagolysosome disruptor. 1-TbAd is highly prevalent among patient-derived *Mtb* strains, where it is among the most abundant lipids produced. Synthesis of TbAd analogs and their testing in cells demonstrate that their biological action is dependent on lipid linkage to the 1-position of adenosine, which creates a strong conjugate base. Furthermore, C20 lipid moieties confer passage through membranes. 1-TbAd selectively accumulates in acidic compartments, where it neutralizes the pH and swells lysosomes, obliterating their multilamellar structure. During macrophage infection, a 1-TbAd biosynthesis gene (*Rv3378c*) confers marked phagosomal swelling and intraphagosomal inclusions, demonstrating an essential role in regulating the *Mtb* cellular microenvironment. Although macrophages kill intracellular bacteria through phagosome acidification, *Mtb* coats itself abundantly with antacid.**

Mycobacterium tuberculosis kills more humans than any other pathogen[1]. Whereas most bacterial pathogens cause acute disease, *Mtb* usually undergoes a years-long infection cycle. *Mtb* persists in humans in part through parasitism of macrophage phagosomes. Survival in this intracellular niche is accomplished by slowing phagosomal maturation and reducing intracellular killing mechanisms[2–4], while offering partial cloaking from immune cells and access to lipids and other host nutrients[5,6]. As *Mtb* interactions with the host play out over years and at diverse anatomical sites, pinpointing specific events that determine tuberculosis (TB) disease outcome is challenging. However, a successful approach has been the comparative profiling of mycobacteria of varying virulence to discover factors selectively present in highly virulent species. *Mycobacterium* species naturally differ in their potential to infect, persist and cause TB, and transmit among hosts. With an estimated 1.7 billion infections worldwide[1], only *Mtb* has broadly colonized the human species, and humans represent its only natural host. These observations highlight the need to identify factors selectively expressed in *Mtb* but not in other mycobacterial species.

Comparative genomics and transcriptomics of *Mtb* and Bacille Calmette-Guèrin (BCG) have isolated factors selectively present in *Mtb*, such as the ESX-1 transporter[7]. Whereas genetic techniques are widely used, comparative chemical biology screens are uncommon in mycobacteria. An HPLC–mass spectrometry (MS)-based lipidomics platform was developed for analysis of all chloroform/methanol-extractable mycobacterial lipids[8,9]. Comparative lipidomics of *Mtb* and BCG identified a previously unknown, *Mtb*-specific lipid missed by genomics approaches: 1-tuberculosinyladenosine (1-TbAd, **1**)[10]. Cyclization of geranylgeranyl pyrophosphate into tuberculosinyl pyrophosphate occurs via the enzyme, Rv3377c, and tuberculosinyl transferase (Rv3378c) generates 1-TbAd, which can chemically rearrange to N^6-TbAd (**2**)[10–12]. So far 1-TbAd has been detected only in *Mtb*[12], so its expression correlates with evolved virulence. However, 1-TbAd has been studied only in laboratory-adapted strains[12,13], and the extent to which it is produced by patient-derived *Mtb* strains remains unknown.

Furthermore, 1-TbAd's function remains unknown. Transposon inactivation of *Rv3377c* or *Rv3378c* reduced *Mtb* uptake, phagosomal acidification and killing of *Mtb* in mouse macrophages[14]. Therefore, 1-TbAd might influence some aspects of these processes in host cells. However, any host receptor, receptor-independent mechanism or other target of 1-TbAd in host cells remains unknown. Commonly used bioinformatic predictors were not helpful for understanding 1-TbAd function, because it was not possible to identify orthologous biosynthetic genes or similar 1-linked purines in other species. Therefore, diverse candidate mechanisms

[1]Division of Rheumatology, Immunology and Allergy, Brigham and Women's Hospital, Harvard Medical School, Boston, MA, USA. [2]Infectious Diseases and Immunity in Global Health, McGill University Health Centre Research Institute, McGill International TB Centre, Montreal, Canada. [3]Electron Microscopy Center Amsterdam, Department of Medical Biology, Amsterdam UMC, Amsterdam, the Netherlands. [4]Department of Chemistry, University of Illinois at Urbana–Champaign, Urbana, IL, USA. [5]Stratingh Institute for Chemistry, University of Groningen, Groningen, the Netherlands. [6]Department of Immunology and Infectious Diseases, Harvard T. H. Chan School of Public Health, Boston, MA, USA. [7]Department of Microbiology and Immunology, Weill Cornell Medical College, New York, NY, USA. [8]Socios en Salud Sucursal Peru, Lima, Peru. [9]Department of Global Health and Social Medicine, Harvard Medical School, Boston, MA, USA. [10]Department of Chemistry, Brandeis University, Waltham, MA, USA. [11]Department of Molecular Biology and Microbiology, Tufts University School of Medicine, Boston, MA, USA. [12]These authors contributed equally: Jeffrey Buter, Tan-Yun Cheng, Adriaan J. Minnaard, D. Branch Moody. *e-mail: bmoody@bwh.harvard.edu

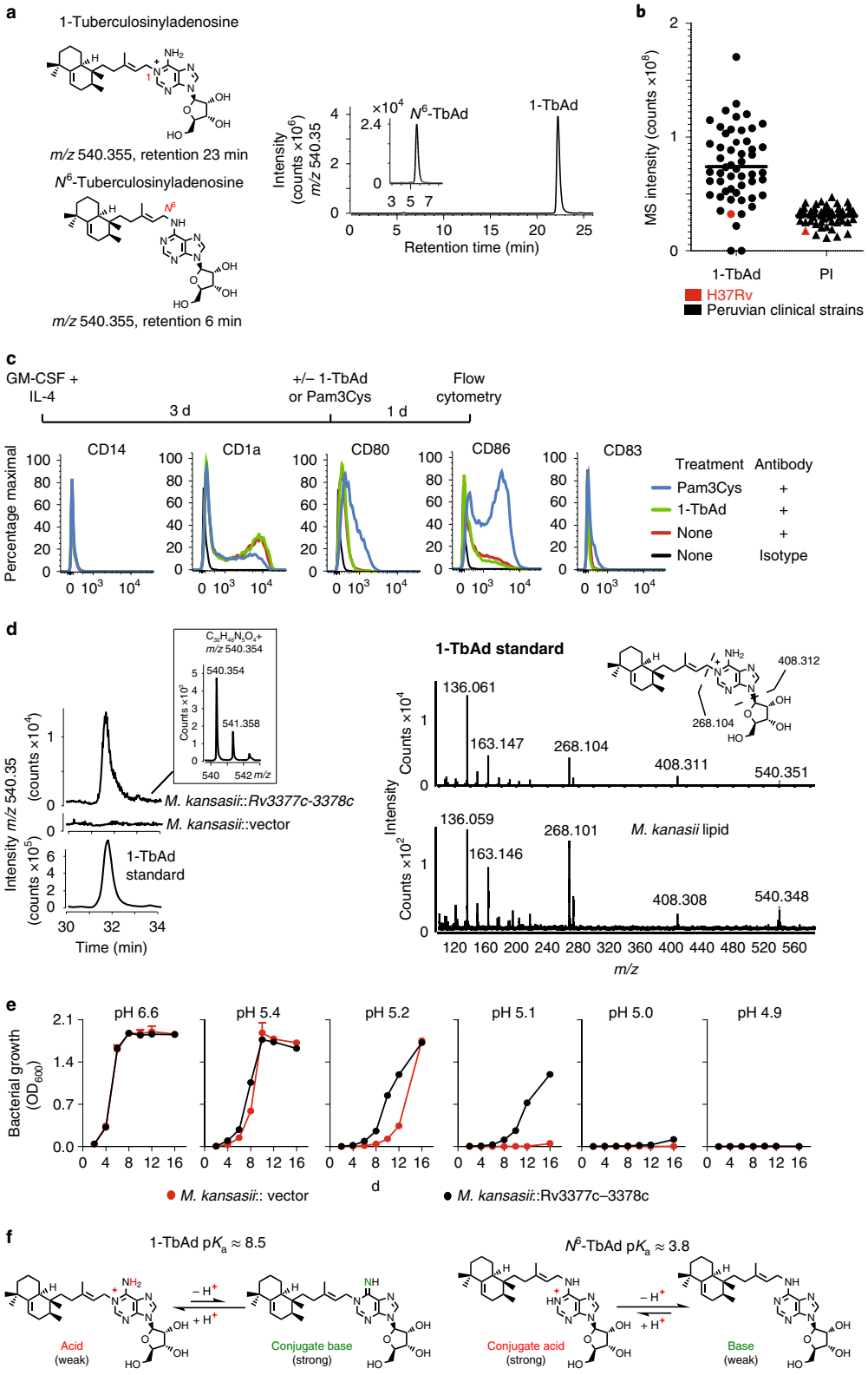

Fig. 1 | Testing signaling-dependent and signaling-independent effects of TbAd on human cells. a, 1-TbAd and N^6-TbAd were detected as HPLC–MS ion chromatograms. **b**, Raw MS counts for 1-TbAd and PI were measured in 52 clinical strains and the laboratory strain H37Rv. **c**, Human monocytes were treated with cytokines followed by a TLR2 agonist (Pam3Cys) or 1-TbAd, and subjected to flow measurement of activation markers in three independent experiments showing similar results. **d**, The *Rv3377c–Rv3378c* locus was transferred into *M. kansasii*, conferring production of a molecule with equivalent mass, retention and the CID mass spectrum fragments found in 1-TbAd. **e**, *M. kansasii* was grown in liquid media at various pH values in duplicate with low variance (coefficient of variation <2% for all but one measurement) in three independent experiments. **f**, The pK_a values are derived from measurements of dimethylallyladenosine and related compounds[21,22], which indicate that 1-TbAd is predominantly charged but in equilibrium with its uncharged conjugate base at neutral pH. Thus, 1-TbAd, but not N^6-TbAd, exists as a strong conjugate base.

of 1-TbAd action were tested on human cells. Unexpectedly, 1-TbAd acts as an antacid that directly protects *Mtb* from acid pH and physically remodels *Mtb* phagolysosomes. Whereas *Mtb* was previously known to resist acidification via exclusion of lysosomal fusion with infected phagosomes[4,6,15], in the present study it is proposed that *Mtb* also resists its normally acidic microenvironment by shedding massive quantities of antacid.

Results

High prevalence of 1-TbAd among clinical *Mtb* strains. 1-TbAd was identified in the laboratory strain H37Rv[10–12]. To determine whether 1-TbAd is produced in patient-derived *Mtb* strains, 52 sputum isolates from Peruvian TB patients were cultured. Complex lipid extracts were subjected to positive-mode HPLC–MS, in which ion chromatograms matching the mass (*m/z* 540.4) and retention time values of 1-TbAd (23 min) and N^6-TbAd (6 min) tracked key compounds (Fig. 1a, and see Supplementary Fig. 1a). Using phosphatidylinositol (**3**) (PI, *m/z* 870.6) as a loading control, strong signals for 1-TbAd were detected in 50 of 52 patient-derived *Mtb* strains (Fig. 1b), leading to several conclusions: 1-TbAd is highly prevalent (96%) but not universally present among strains. Among the 50 1-TbAd$^+$ strains, mean 1-TbAd signals were higher than for PI, an abundant membrane lipid. Patient-derived strains expressed 1-TbAd at higher mean intensity (78×10^6) than strain H37Rv (31×10^6), indicating that prior studies on laboratory strains[10,12] underestimated production by clinical strains.

Extending a prior study that detected 1-TbAd only in *Mtb*[12], a basic local alignment search tool analysis identified orthologs of *Rv3377c* and *Rv3378c* only in species highly related to *Mtb*. We did not identify species with orthologs among environmental mycobacteria distant from the *Mtb* complex or any other bacterium, including common non-mycobacterial lung pathogens (see Supplementary Fig. 1b). Although these genetic results do not rule out convergent evolution of TbAd-like molecules based on unrelated genes, the probable conclusion is that TbAd biosynthesis is restricted to virulent mycobacterial species. *Mtb*-specific expression of TbAd biosynthesis genes and broad clinical prevalence of 1-TbAd provided a strong rationale to determine TbAd's function.

TbAd biosynthetic genes in pH regulation. Macrophages are host cells for *Mtb* residence and play key roles in killing *Mtb*[4]. The known roles of adenosine and other purinergic receptors on macrophages and the adenosine moiety in TbAd[16,17] led to testing of its activating properties on mixed human myeloid cells. However, 1-TbAd did not alter markers of monocytes (CD14), activation (CD80, CD86) or maturation (CD1a, CD83), which tested MyD88, mitogen-activated protein kinase and other activation pathways (Fig. 1c). Quorum sensing was considered, but no correlation was found between 1-TbAd concentrations and growth (see Supplementary Fig. 1c).

Based on the observed high 1-TbAd production (Fig. 1b) and reinterpretation of a transposon screen showing that *Rv3377c* and *Rv3378c* controlled *Mtb* phagosomal acidification[14], it was hypothesized that 1-TbAd might act as an exotoxin that controls the pH of phagolysosomes. This hypothesis was plausible because only *Mtb* blocks phagosomal acidification[4], and only *Mtb* is known to produce 1-TbAd[12] (see Supplementary Fig. 1b). Two landmark studies previously showed that *Mtb* blocks vesicular ATPase (vATPase) fusion with infected phagosomes[2,3]. This deacidification mechanism is now considered a central means of evasion of cellular killing by macrophages. Resetting the pH from 5 to 6.2 inhibits downstream antibacterial effector functions[15,18], including acid hydrolases, and reactive oxygen and nitrogen intermediates[4,19], as well as autophagy, which is a major cellular pathway controlling *Mtb* survival[20].

In contrast to deacidification via vATPase exclusion[2,3], two observations indicated that TbAd probably operated via a previously unknown mechanism. First, *Rv3377c–Rv3378c* was transferred into *M. kansasii*, which conferred biosynthesis of a molecule with the mass, retention time and collision-induced dissociation (CID) mass spectrum (Fig. 1d) of 1-TbAd. Gene transfer did not affect growth in media at neutral pH, but did increase survival under pH stress (Fig. 1e). Increased growth was observed at pH 5.4–5.1, which can be achieved in activated macrophages, but is not found during virulent *Mtb* infection, where the pH is 6–6.2 (ref. [6]). Decreased *Mtb* survival after knockout of *Rv3377c–Rv3378c*[14] and increased survival after *Rv3377c–Rv3378c* knock-in to *M. kansasii both* represented strong links of TbAd biosynthetic genes with mycobacterial growth and survival. Importantly, the *M. kansasii* experiment indicated that TbAd biosynthetic genes act on *Mtb* itself, so key effects occurred independently of vATPases and all other host cell factors. A second clue to a possible function is that 1-TbAd is a strong conjugate base, so it has intrinsic antacid properties. Model compounds[21,22] indicate that the pK_a of 1-TbAd is ~8.5. The lipid linkage to the 1-position of adenosine renders the molecule acidic and therefore in equilibrium with its conjugate base, which is a strong base (Fig. 1f). Thus, the abundant shedding of 1-TbAd into the extrabacterial space[10] could act as an antacid, locally neutralizing the acidic phagolysosomal microenvironment.

Massive biosynthesis of 1-TbAd by *Mtb*. Unlike receptor-mediated amplification, base-mediated pH neutralization is stoichiometric: one molecule of basic 1-TbAd captures one proton (Fig. 1f). De novo synthesis of 1-TbAd requires 26 steps (see Supplementary Fig. 2), so neutralization of pH by ~0.7 pH units would be metabolically expensive. Mitigating this concern, *Mtb* strains showed high absolute MS signals (Fig. 1b) and produce 1-TbAd constitutively under many conditions[10,11], and at low and high bacterial density (see Supplementary Fig. 1). The pH-dependent effector molecules in phagolysosomes are directly adjacent to intracellular mycobacteria, and phagosomes have a small volume (~10^{-15} l) (**23**). Thus, effective pH neutralization could plausibly be generated in close proximity to *Mtb*.

To assess whether 1-TbAd biosynthesis was quantitatively sufficient for its proposed cellular effect, 1-TbAd was measured among additional patient-derived *Mtb* strains. Thin-layer chromatography of total lipids from three TbAd$^+$ but not TbAd$^-$ strains showed dark spots with the same retention factor as the 1-TbAd standard (0.51). This spot was among the darkest spots seen in total *Mtb* lipid extracts (Fig. 2a). After synthesis of 1-[$^{13}C_5$]TbAd (**4**) (*m/z* 545.374) as an internal standard (Fig. 2b), quantitative analysis demonstrated that 1-TbAd comprised ~1% of total *Mtb* lipids in clinical strains (Fig. 2c). Approximately 7 ng of 1-TbAd was measured per 10^8 bacteria, with 91% cell-associated and 9% shed (Fig. 2d). Assuming one bacterium per phagosome[23], intraphagosomal concentrations could plausibly reach micromolar concentrations and cause ~0.7 pH unit effect (see Supplementary Fig. 3)[6,14]. Overall, these experiments document massive biosynthesis and accumulation, establishing 1-TbAd as one of the most abundant *Mtb* lipids.

Influence on lysosomal pH in cells. Next, 1-TbAd's effect on phagocytosis and lysosomal pH was tested in macrophage-like (THP-1) cells. As trace contaminants in *Mtb*-derived 1-TbAd can confound cellular assays, 1-TbAd was synthesized as well as nine analogs (compounds **5**–**12**) for testing in parallel with *Mtb*-derived material[24] (Fig. 3a, and see Supplementary Fig. 4). LysoTracker is a red fluorescent dye that accumulates in acidic compartments. Pre-feeding cells with green fluorescent beads allows concomitant measurement of phagocytosis (see Supplementary Fig. 5). Green beads were rarely seen outside the perimeter of cells in diffraction interference contrast images and could be excluded when present (see Supplementary Figs. 5, left panels, 6a). To assess cellular entry, a pilot study showed that ~81% of beads were ringed with lysosomal-associated membrane protein 1 (LAMP-1) staining and that 1-TbAd pre-treatment

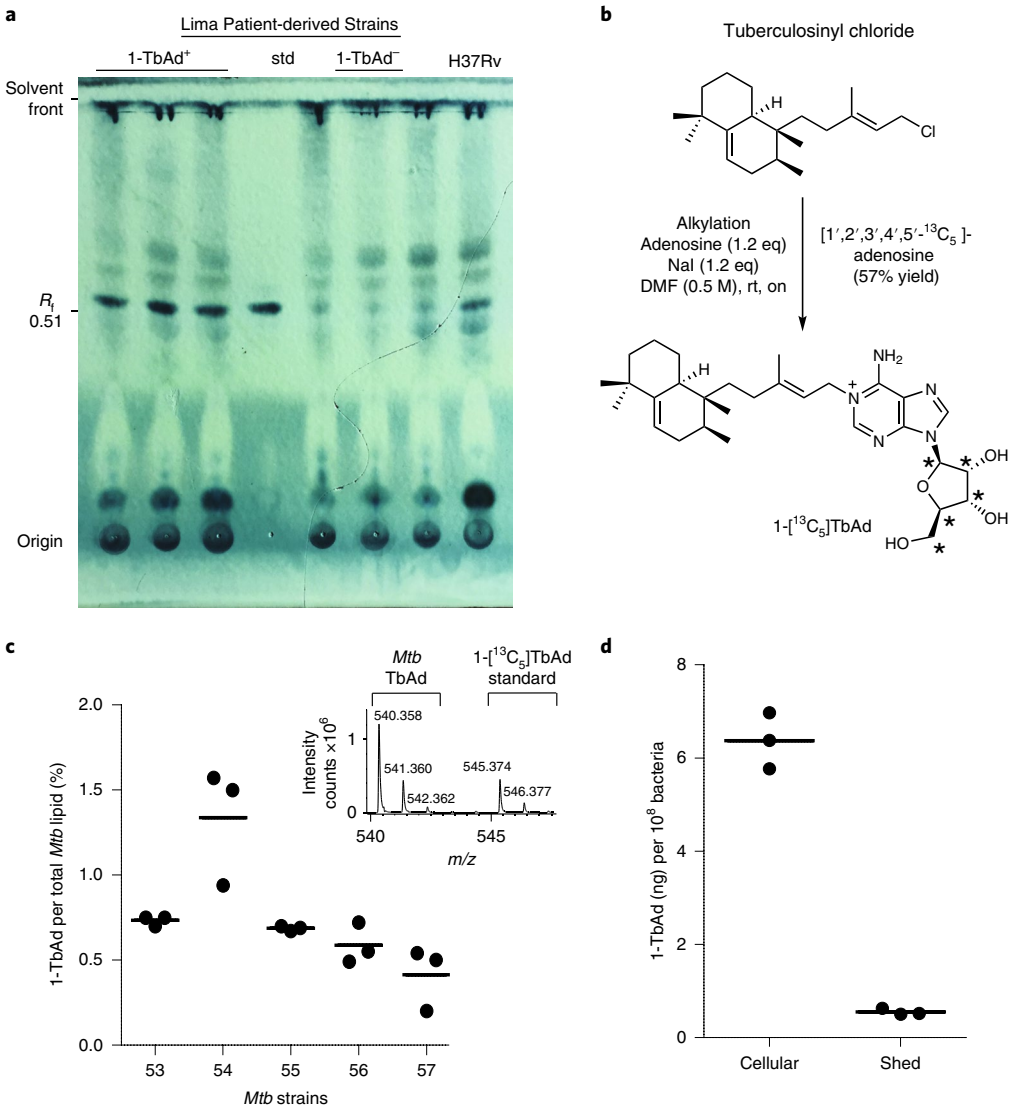

Fig. 2 | Quantitative measurements of 1-TbAd using an internal standard on a per cell basis. a, Total lipids from three 1-TbAd$^+$ and three 1-TbAd$^-$ strains were separated on normal-phase, silica, thin-layer chromatography using chloroform/acetic acid/methanol/water mixtures compared against a 1-TbAd standard and a H37Rv lab strain. Lipids were subjected to charring after spraying with a phosphomolybdic acid solution. R_f, retention factor. **b**, Labeled 1-TbAd was synthesized using $^{13}C_5$-labeled adenosine with mass spectral peaks that did not overlap with those of natural 1-TbAd, allowing its use as an internal control. **c**, Total lipids from five patient-derived *Mtb* strains were weighed and subjected to HPLC–MS measurement in triplicate using the ^{13}C-labeled internal standard to provide absolute mass values, which were expressed as the percentage of input lipid from three biologically independent samples. **d**, For one representative clinical strain, lipids were extracted from the cell pellet (cellular) or conditioned media (shed) and measured as in **c**, expressed on a per-cell basis based on colony-forming unit measurements from the input culture. std, standard; DMF, dimethylformamide; rt, room temperature; on, overnight.

did not alter this ratio (see Supplementary Fig. 6a). For the larger study with seven tested compounds (see Supplementary Fig. 5), fluorescence results from five fields (>100 cells) showed similar results in three assays (see Supplementary Fig. 6b). Using total bead uptake as a measure of phagocytosis, no statistically significant changes were found in any condition. For measurement of lysotracker$^+$ compartments, two negative controls, phosphatidylcholine (**13**) and isotuberculosinol (**14**), showed no effect. Both natural and synthetic 1-TbAd notably reduced the number of lysotracker$^+$ compartments (Fig. 3b, and see Supplementary Figs. 5 and 6b). 1-Phytyladenosine (**5**), which contains a straight-chain polyprenyl group substituted for the ringed tuberculosinyl unit in 1-TbAd, showed a similar effect, indicating that the halimane core is not essential. Adenosine (**15**) and N^6-TbAd, which lack the 1-linkage that confers proton capture (Figs. 1f and 3b), had no effect on lysotracker staining.

Extending this preliminary study of THP-1 cells, studies of primary mouse bone marrow macrophages treated with carboxyfluorescein were undertaken. The latter approach allows more direct assessment of pH through comparison of fluorescence at pH-dependent (excitation 490 nm, emission 520 nm) and pH-independent (excitation 450 nm, emission 520 nm) wavelengths[25]. Feeding carboxyfluorescein silica beads to fresh macrophages provides a readout of relative pH as phagosomes mature over time[26]. 1-TbAd and chloroquine (**16**), a positive control for a lysosomotropic base, showed similar outcomes. Chloroquine provided a more rapid effect, but slightly lower peak effect on baseline fluorescence (Fig. 3c). Control wells with beads treated with 1-TbAd demonstrated the lack of direct effect on fluorescence (Fig. 3d). In wells with macrophages, addition of 1-TbAd and 1-phytyladenosine (**5**) delayed and reduced acidification of phagosomes in a concentration-dependent

manner, whereas adenosine had little effect (Fig. 3d). Overall, in human and mouse cells, the outcomes of two pH assays matched the prediction that 1-linked but not N^6-linked adenosines could raise the pH. The role of C_{20} lipid moieties was hypothesized to provide the hydrophobicity needed to traverse membranes. However, assays in live cells do not establish this conclusion because compounds could have been actively ingested.

Lysosomotropism predicts TbAd behavior. These clear structure–activity relationships (SARs) were combined with descriptions of lysosomotropic drug behavior by de Duve et al.[27] to generate a detailed model for 1-TbAd function (Fig. 4a)—TbAd is in equilibrium with its uncharged conjugate base (Fig. 1f), which is proposed to permeate mycobacterial membranes to reach the phagosomes (Fig. 4a, and see Supplementary Fig. 7). In an acidic environment (pH 5.5–6.2), 1-TbAd ($pK_a \approx 8.5$) but not N^6-TbAd ($pK_a \approx 3.8$) neutralizes pH, creating 1-TbAd$^+$, a charged, membrane-impermeable species that is trapped (see Supplementary Fig. 7a). Intraphagosomal protonation is predicted to generate a concentration gradient of uncharged base across the mycobacterial membrane, where permeation and trapping continue until equilibrium is reached. This process is proposed to create a large intraphagosomal pool of 1-TbAd$^+$, the relative size of which is predicted by the Henderson–Hasselbalch equation (Fig. 4a, and see Supplementary Fig. 7b). Although extracellular drugs, such as chloroquine, cross membranes into cells and enter lysosomes[27], the reverse topology is proposed here: natural molecules made in the mycobacterial cytosol escape outwards and are trapped within maturing phagosomes (see Supplementary Fig. 7c).

High-throughput screens[28] and lysosomotropic models[27] emphasize that a $pK_a \approx 8$, as in the case of 1-TbAd, is optimal for lysosomotropism. Compounds with substantially higher pK_a values remain charged and impermeant, whereas those with lower pK_a values, such as N^6-TbAd, permeate membranes but do not efficiently capture protons (see Supplementary Fig. 5). These models led us to more extensively compare 1-TbAd function with chloroquine, a known lysosomotropic base[27]. Chloroquine is widely used against malaria, systemic lupus erythematosus and other autoimmune diseases. These medical indications rely on its lack of signaling, low toxicity and tropism to lysosomes[29]. In experimental medicine, chloroquine's antacid effects block antigen presentation by major histocompatibility complex class II (MHC-II), toll-like receptor activation and autophagy[29].

EM of human macrophages. In EM, macrophage lysosomes appear as highly electron-dense structures (Fig. 4a, and see Supplementary Fig. 8a,b). Chloroquine or 1-TbAd transformed these small, electron-dense compartments into large, electron-lucent compartments that, despite complete loss of their multilamellar and electron-dense appearance, could still be recognized as lysosomes based on immunogold staining of CD63, a lysosome marker (Fig. 4b,c, and see Supplementary Fig. 8). This process was widespread (Fig. 4b, and see Supplementary Fig. 8a,c,e), such that cells were designated as having swollen lysosomes when the electron-lucent compartments involved more than one-third of the cytoplasm (Fig. 4b). Both the nature of intraphagosomal inclusions and the broad extent of cellular involvement are visualized through side-by-side comparison of low- and high-magnification images with pseudocoloring of lysosomes (see Supplementary Fig. 8). By analysis of >100 cells per condition, 1-TbAd showed statistically significant effects on lysosomes compared with no treatment (Fig. 4b).

For chloroquine this structural transformation is known to involve its accumulation in acidic compartments and secondary osmotic effects[20,27,29]. 1-TbAd showed stronger effects than chloroquine on human macrophages (Fig. 4b). The lysosomotropic model predicts that non-acidic organelles, such as early endosomes, Golgi bodies and mitochondria, would be relatively unaffected[27], as observed in the assays in the present study (Fig. 4d). For chloroquine and 1-TbAd the appearance of small, mildly electron-dense inclusions was noted, including membrane-containing intralysosomal bodies (Fig. 4e, and see Supplementary Fig. 8), which, for chloroquine, results from autophagy blockade[20,27,29]. Last, a negative control, tuberculosinol (**17**), produced no discernible effects on lysosomes, again suggesting the importance of the 1-adenosine linkage (see Supplementary Fig. 9).

Testing vesicle permeation. Lysosomotropism requires membrane permeation (Fig. 4a), but lysotracker suppression in THP-1 cells (Fig. 3b) and macrophages (Fig. 3d) might have occurred through active cellular uptake. To measure transmembrane diffusion, the present study took a look at model membrane systems. For inverted membrane vesicles (IMVs)[30], inversion orients proton pumps so that the interior spontaneously acidifies in response to added energy substrates, ATP or succinate. The reporter, 9-amino-6-chloro-2-methoxyacridine, is quenched by acid. Quenching is reversed by penetration of lysosomotropic substances into the IMV. Compounds that disrupt membranes cause decreased fluorescence, providing a control for membrane leakage[30]. Unlike cells (Figs. 3 and 4, and see Supplementary Fig. 5), IMVs have no active cytoskeleton-mediated drug uptake. As a positive control, chloroquine showed reporter quenching with half-maximal effect at ~20 μM, matching its expected function and potency[27–29] (Fig. 5a).

All four 1-linked adenosines (**1**, **5**–**7**) carrying C_{20} lipids were more potent than chloroquine, and none of the N^6-linked adenosines (**2**, **11**, **12**) showed suppression (Fig. 5a). These results suggest direct membrane permeation and rule in the 1-linkage as the essential chemical feature (Fig. 4a). Stereochemical changes in the 1-linked lipid ((*Z*)1-TbAd) (**7**), or an acyclic lipid (1-phytyladenosine, **5**), had little effect, as long as a C_{20} lipid was present. However, C_{10}, C_5 or C_1 lipid analogs (**8**–**10**) showed that potency declines as chain length decreases, consistent with the lipid moiety generating a hydrophobic effect (Figs. 3a and 5a). Carbohydrate-modified, 2′-deoxy-1-TbAd (**6**), was more potent than 1-TbAd and chloroquine. Thus, hydrophobicity and potency are correlated among analogs. This result suggests that hydrophobicity drives biological action and provides an approach to future synthesis of yet more potent compounds. Similar results were observed when using ATP or succinate as energy substrates, and using *Mycobacterium smegmatis* or *Escherichia coli* IMVs (Fig. 5a). The SARs in IMVs generally matched the patterns seen in human (Figs. 3b and 4) and mouse cells (Fig. 3c,d).

Prior studies suggested that beads coated with the free alcohol component of TbAd could alter the pH of phagosomes[31]. However, isotuberculosinol (**14**) and tuberculosinol (**17**) are not predicted to have basic properties, and they showed few effects in lysotracker studies (Fig. 3b), EM images (see Supplementary Fig. 9) and *E. coli* IMVs (Fig. 5a). However, IMV assays with *M. smegmatis* membranes (Fig. 5a) did show some effect with synthetic tuberculosinol. These somewhat differing results might be explained if the tuberculosinyl moiety mediates some unknown but specific interaction with mycobacterial membranes.

Protein-free model membranes. To exclude artifacts from inhibitors binding to protein targets in IMVs, testing of protein-free membranes was required. Therefore, we generated liposomes with differing interior pH values (5.0 and 7.4) (Fig. 5b). Lysosomotropism predicts that externally applied compounds selectively penetrate acidic but not neutral liposomes. Fulfilling this prediction, chloroquine co-migrated with acidic but not neutral liposomes on a size-exclusion column. A negative control, adenosine, failed to bind to either liposome type. 1-TbAd and N^6-TbAd showed some adhesion to neutral and acidic liposomes (Fig. 5c), which was probably mediated by their identical lipid moieties (see Fig. 1a). Only 1-TbAd was

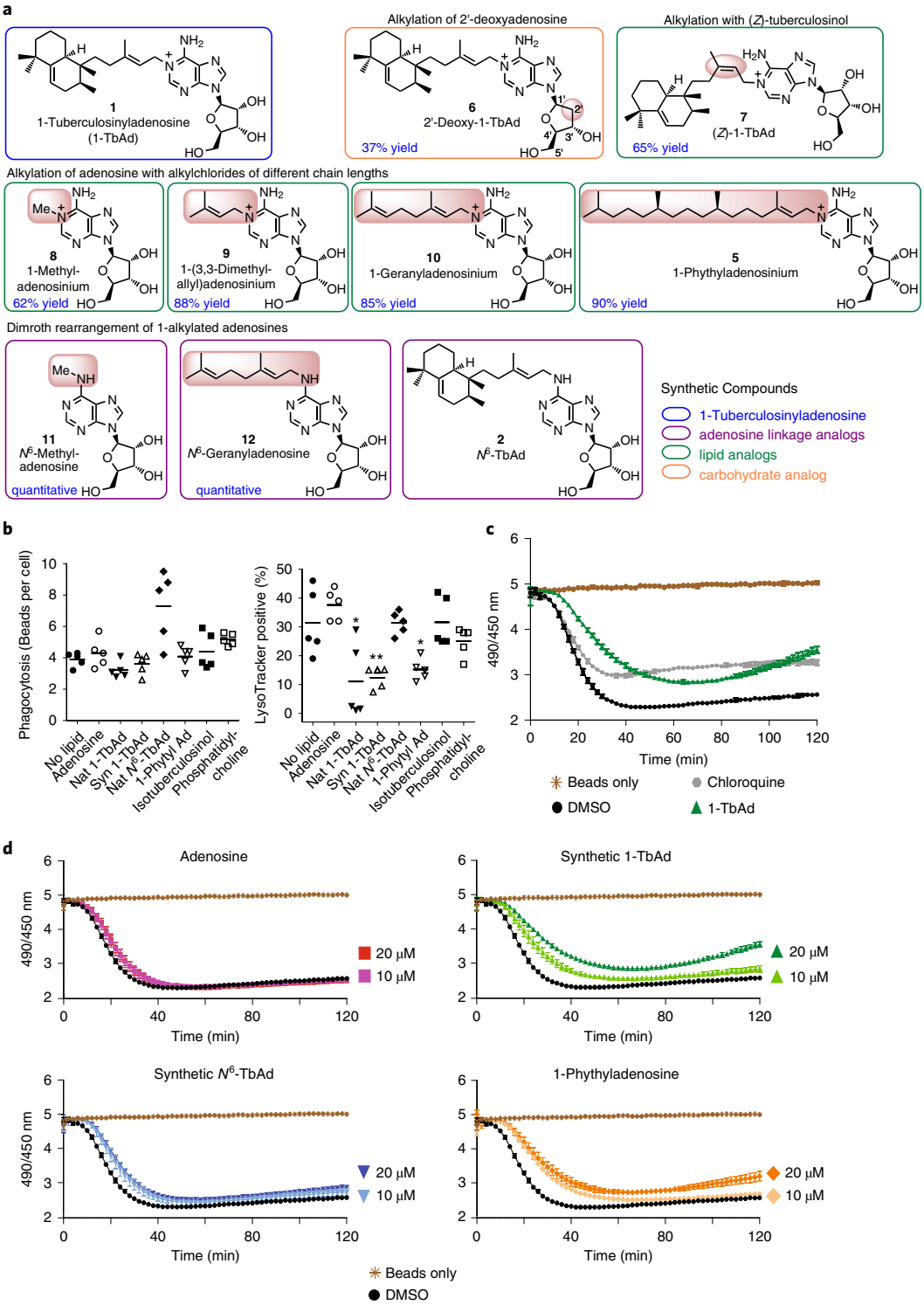

Fig. 3 | Effect of synthetic analogs of 1-TbAd on lysosomal pH in THP-1 cells and macrophages. a, Synthetic 1-TbAd and analogs that differ in the linkage or nature of the lipid or carbohydrate were prepared as described in Supplementary Fig. 4. **b**, Phagocytosis of green fluorescent beads and the pH-sensitive lysotracker dye in human THP-1 cells was monitored by confocal microscopy in three independent experiments, each evaluating five low-power sections with all outcomes shown in Supplementary Figs. 5 and 6. *P* values were calculated using the two-tailed, Student's *t*-test and s.d.s are shown. **c**,**d**, Carboxyfluorescein beads were added to murine bone marrow-derived macrophages seeded in a 96-well plate, or to wells containing only medium, and fluorescence was tracked with a microplate reader every 2 min for 2 h. Compounds at indicated concentrations were added at the start of the assay. Data are shown as mean and s.d. from five or six replicate wells, which represent three independent experiments. 1-TbAd was tested and compared to chloroquine (positive control) and vehicle (DMSO, negative control) (**c**). 1-TbAd, 1-phytyladenosine, N^6-TbAd, and adenosine were subjected in the carboxyfluorescein assay at the indicated concentrations (**d**).

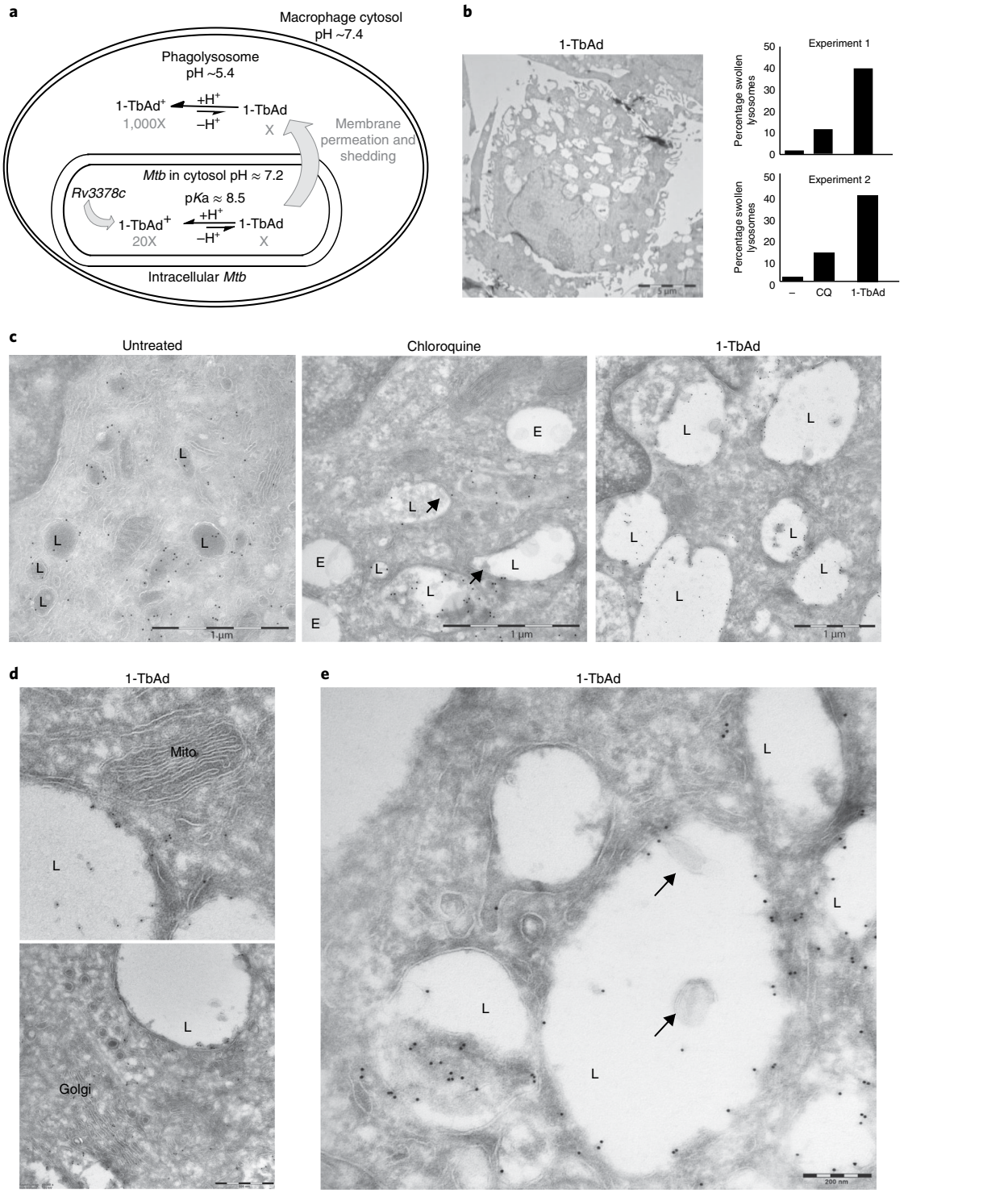

Fig. 4 | 1-TbAd is a lysosomotropic antacid. a, Experiments test a compartmentalization model in which *Rv3378c* generates intrabacterial 1-TbAd, and the uncharged conjugate base permeates membranes. Low pH in phagolysosomes drives protonation, which incrementally raises pH and generates a charged species, 1-TbAd$^+$, which cannot cross membranes. **b**, Human macrophages generated with M-CSF and GM-CSF were treated for 2 h with 1-TbAd (20 μM) or chloroquine (20 μM) stained with anti-CD63 immunogold and assessed by TEM. An individual macrophage was counted as having swollen lysosomes when >30% of cytosol was involved with CD63$^+$ electron-lucent structures, as depicted in this low magnification image of a 1-TbAd-treated cell. Images of >150 cells were counted and subjected to the Cochran–Mantel–Haenszel test and adjusted using the method of Benjamini and Hochberg ($P = 5.4 \times 10^{-10}$ for control versus 1-TbAd and $P = 3.2 \times 10^{-5}$ for chloroquine versus 1-TbAd). Actual sample sizes were $n = 54$ or 48 for controls, $n = 45$ or 48 for 1-TbAd treated and $n = 70$ or 46 for chloroquine treated in trial 1 or 2, respectively. **c**, High magnification images (bar, 1 μm) depict lysosomes (L), as defined by anti-CD63 staining at the limiting membrane, and endosomes (E), which are electron-lucent structures lacking anti-CD63 staining. Results represent three biologically independent experiments with similar outcomes. **d**, Mitochondria (Mito) and Golgi stacks (Golgi) are recognized by membrane arrangements, which, unlike lysosomes, did not show swelling or increased electron lucency. **e**, Higher magnification (scale bar, 200 nm) images show inclusions in lysosomes that contain membranes (arrows) or non-membrane-bound inclusions.

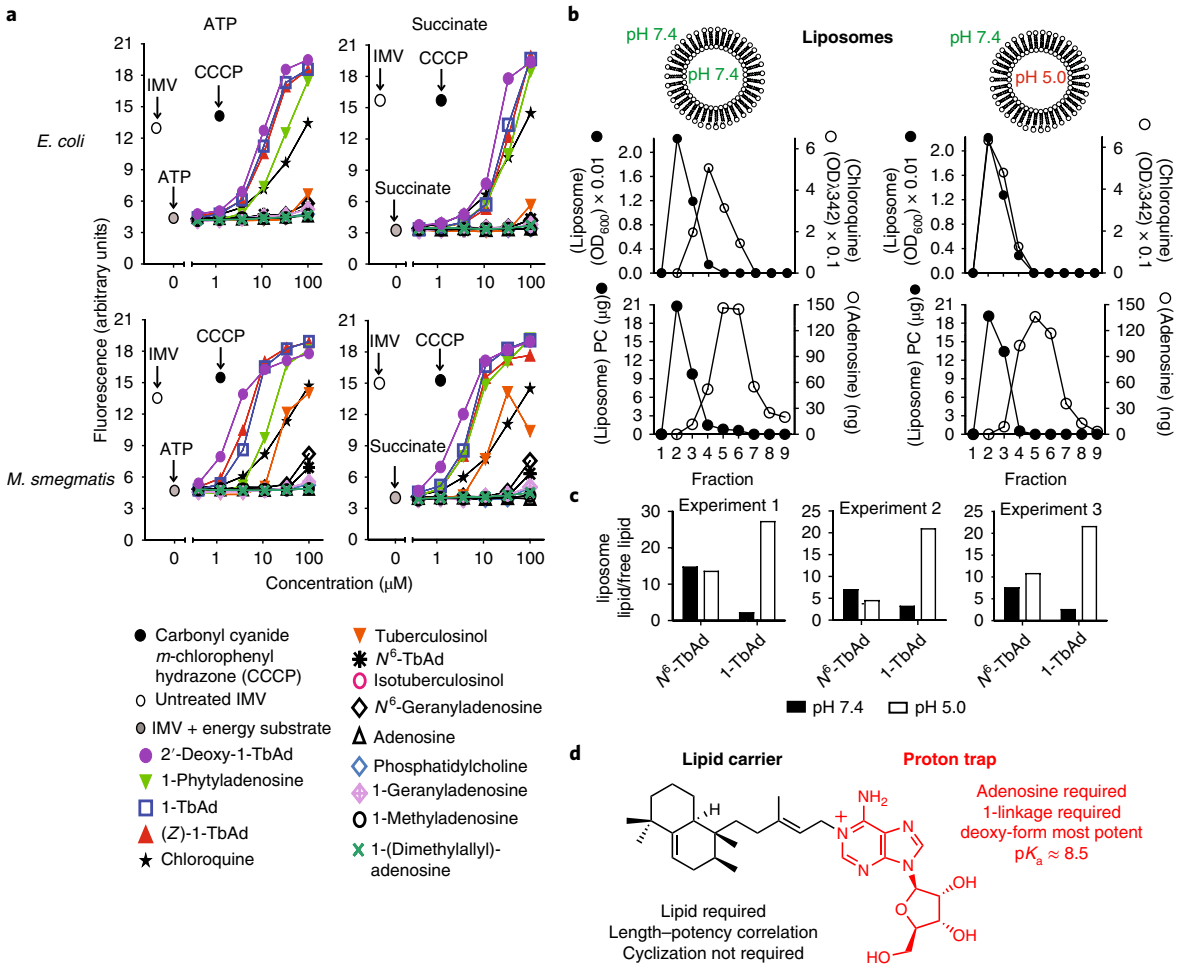

Fig. 5 | Transmembrane permeation by TbAd analogs. a, Fluorescence spectroscopy assays of *E. coli* and *M. smegmatis* (*M. smeg*) IMVs used ATP or succinate to generate a pH gradient, followed by addition of the indicated compound. Four representative assays are shown from a total of six assays that found similar results and were conducted in a blinded fashion. **b**,**c**, Liposomes with a neutral or acidic interior were treated with negative control compounds (adenosine, N^6-TbAd), a positive control (chloroquine) or 1-TbAd, and then subjected to size exclusion chromatography. Phosphatidylcholine (PC) containing liposomes (black) were measured using absorbance at 600 nm and chloroquine was measured at 342 nm. Adenosine-containing compounds were measured using MS. 1-TbAd at pH 5.0 differed significantly from all other treatments ($P < 0.01$) using the least-squares means post-test with adjustment by Tukey's method after fitting a linear model and factorial ANOVA. **d**, Summary of cellular, IMV and liposome-based analysis of TbAd analogs identifies separate roles on the lipid carrier and proton trap site at the 1-position of adenosine.

preferentially captured by liposomes with an acidic interior (Fig. 5c). This reductionist system rules in a purely chemical mechanism: 1-TbAd is a membrane-permeable antacid, where the 1-linked lipid moiety provides intrinsic transmembrane tropism for acidic compartments (Fig. 5d). Overall, 1-TbAd is a naturally evolved phagolysosome disrupter, with an action that mimics the widely used lysosomotropic drug chloroquine.

Generation of *Mtb* lacking *Rv3378c* and 1-TbAd. To identify non-redundant functions of the 1-TbAd biosynthesis pathway during cellular infection, the tuberculosinyl transferase gene, *Rv3378c*, was deleted in the H37Rv strain (*MtbΔRv3378c*) (see Supplementary Fig. 10a). Gene deletion and replacement with the hygromycin-resistance cassette were confirmed through PCR analysis, as well as the complete abrogation 1-TbAd biosynthesis (see Supplementary Fig. 10b). For genetic complementation (*MtbΔRv3378c::Rv3378c*), a single-copy chromosomal integration of *Rv3378c* was used under the control of a mycobacterially optimized promoter. Full restoration of 1-TbAd production to wild-type levels was observed after subculture and selection of a high producing *Mtb* clone (see Supplementary Fig. 10b).

Role of biosynthetic genes in live macrophage infection. After 4 d of infection, human macrophages were examined by transmission EM (TEM). High magnification images depicting transbacterial sections revealed infected phagosomes. Transverse sections show that mycobacterial cytosol (*) is surrounded by the cell wall, phagosomal space, limiting phagosomal membrane and macrophage cytosol (Fig. 6a). For *MtbΔRv3378c*, most intraphagosomal bacteria were surrounded by an electron-lucent ring of uniform thickness (~20 nm), the mycobacterial polysaccharide capsule (Fig. 6a, small arrows)[32]. For *MtbΔRv3378c* the phagosomal membrane is typically tightly wrapped around the 20-nm mycobacterial capsule (tight phagosome).

In contrast, for wild-type *Mtb*, phagosomal membranes typically showed numerous large (~20–250 nm) ectopic blebs (Fig. 6a, large arrows) outside the capsular ring. In some cases these blebs almost surround the bacterium, creating the appearance of a loosely wrapped (swollen) phagosome with many non-bacterial, intraphagosomal inclusions. Inspection of >150 phagosomes in each of two experiments showed that *Rv3378c* expression resulted in a 4.5- or 4.9-fold increase in the ratio of swollen to tight phagosomes (Fig. 6b). The swollen phagosomes provided clear evidence for

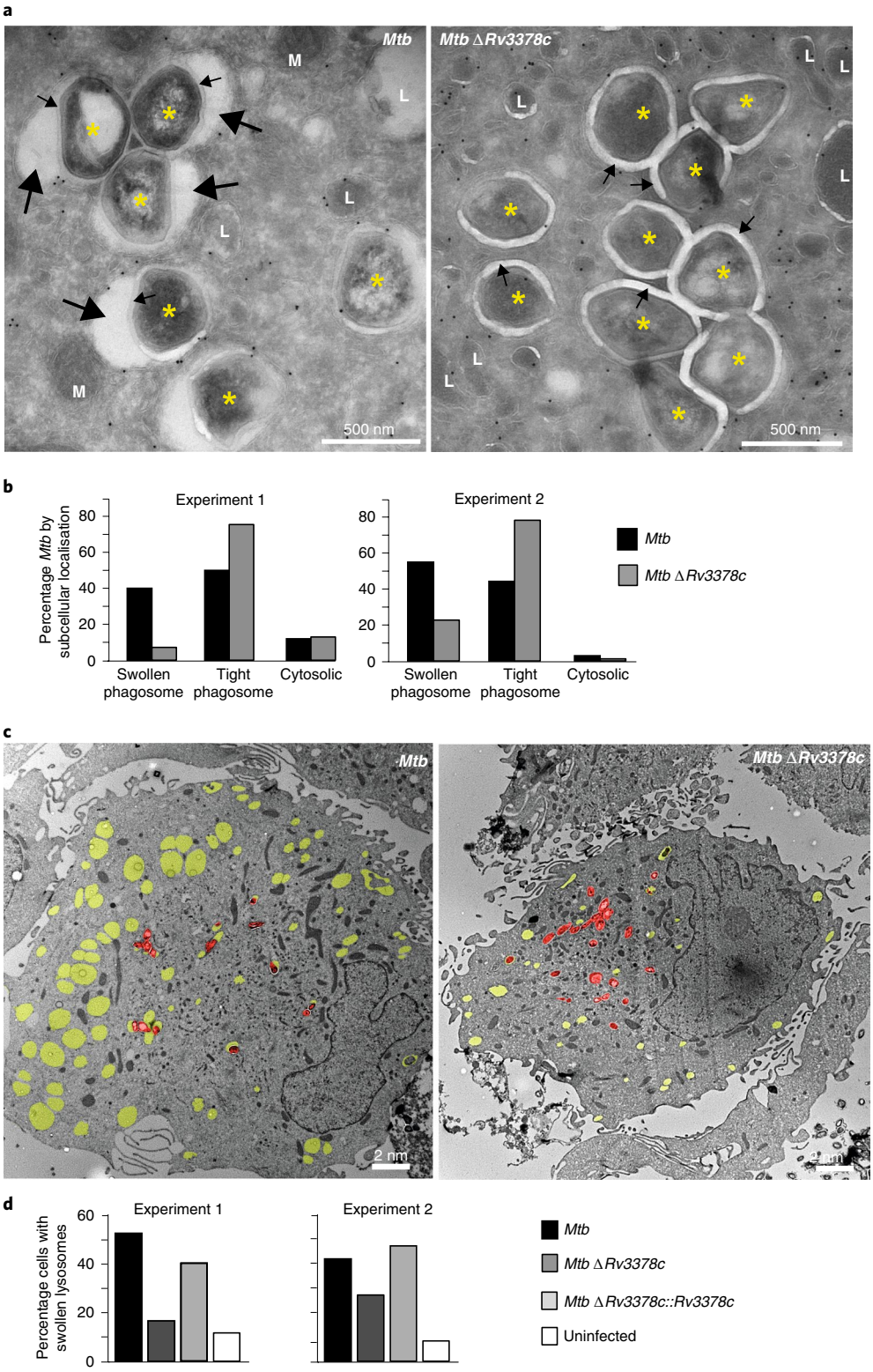

Fig. 6 | Infection of human macrophages for 4 d with *Mtb* or the *Rv3378c*- deletion mutant, which lacks TbAd production. a, High magnification images of macrophage cytosol containing *Mtb* (*), mitochondria (M), lysosomes (L), capsular layer (small arrow) or intraphagosomal area with inclusions (large arrow). **b**, More than 150 intracellular *Mtb* bacilli were evaluated at high power for their localization in the cytosol, tight phagosomes (small arrows) or large phagosomes ($P = 7.0 \times 10^{-15}$ for swollen versus tight phagosomes). **c**, Low-magnification images show yellow pseudocoloring for swollen lysosomes (CD63 immunogold, electron lucent) and red pseudocoloring highlights individual *Mtb* bacilli. **d**, More than 150 cells were evaluated as having swollen lysosomes when one-third of the cytosolic area showed electron-lucent CD63$^+$ compartments ($P < 0.001$ for *Mtb* versus *MtbΔRv3378c*; $P < 0.05$ for *MtbΔRv3378c* versus *MtbΔRv3378c::Rv3378c*). All *P* values in **b** and **d** were calculated using the Cochran–Mantel–Haenszel test with independent experiments treated as strata and were adjusted using the method of Benjamini and Hochberg.

compartment autonomous effects of *Rv3378c* expression (Fig. 4a). Low-power analysis revealed that expression of *Rv3378c* was associated with many swollen phagosomes that lacked visible bacteria (Fig. 6c). The broader involvement of compartments was somewhat surprising, because it suggested that 1-TbAd produced in one compartment could more broadly affect lysosomes in cells.

Therefore, more detailed and quantitative analysis was undertaken of low-magnification images of infected cells with visible bacteria (Fig. 6c, red pseudocolor). Individual cells were scored as having swollen lysosomes when one-third of the cytosol was involved (Fig. 6c, yellow pseudocolor). Compared with uninfected macrophages, *Mtb*-infected human macrophages showed marked increases with swollen lysosomes (Fig. 6d). *Rv3378c* deletion significantly reduced swelling, and complementation restored the phenotype to the baseline value. Although undetected bacteria cannot be ruled out in swollen lysosomes, the multiplicity of infection used (two bacteria per cell) and the large number of swollen compartments suggested non-compartment autonomous effects. It was concluded that effects downstream of *Rv3378c* play an essential role in the physical remodeling of the local intraphagosomal growth niche of *Mtb*. Phenotypes from wild-type *Mtb* (Fig. 6) mimicked key aspects seen after treatment with pure 1-TbAd (Fig. 4c–e), and they match the predicted effects of release of any lysosomotropic substance[27] and the known effects of chloroquine[29].

Discussion

Based on 1-TbAd's shed nature and restriction to virulent mycobacteria in the *Mtb* complex, initially comparisons were considered with bacterial endotoxins and exotoxins, such as lipopolysaccharide, which mediates rapid and extreme host cellular response. Although no experiment can rule out receptor-mediated signaling, no evidence for generalized cellular activation was found in response to 1-TbAd. Mechanistically, increased growth of 1-TbAd$^+$ *M. kansasii* at acidic pH is critical, because it rules in macrophage-independent effects on mycobacterial growth and specifically connects survival to pH. Rather than a generalized cellular toxin, 1-TbAd is a lysosomotrope, causing gross phagosome disruption and raising the pH in THP-1 cells and macrophages. This conclusion is strengthened by comparison to the known lysosomotrope, chloroquine[27,29], as well as consistent patterns among TbAd analogs that directly implicate the 1-linkage, which confers its antacid property.

Thus, 1-TbAd mediates a previously unknown effect involving neutralization and local remodeling of *Mtb*'s intracellular acidic growth niche within macrophages. As 1-TbAd is initially released only at the surface of live mycobacteria, the model predicts the strongest effects within infected phagolysosomes. Therefore, finding broadly swollen lysosomes, including many compartments with no detectable bacilli, was initially surprising. However, the reverse lysosomotropic model allows that steady production over time by intracellular bacteria could lead to 1-TbAd penetration to all acidic compartments, a hypothesis that can now be tested with kinetic studies.

Massive production of 1-TbAd, among 96% of tested patient strains, is notable. Extending work in which TbAds were detected in mice[12], these findings support the feasibility of developing 1-TbAd as a marker of *Mtb* infection and TB disease. Also, the high production among patient strains highlights one surprising aspect of this work[12], which is the failure of such an abundant molecule to be detected during decades of TB research. Overall, the high biosynthesis is well matched to an unamplified, stoichiometric mechanism of action that involves proton capture.

Modified adenosines and related purines have evolved repeatedly in eukaryotic and prokaryotic cells, but 1-linked adenosines are rare in nature[10,33]. Such adenosines can non-enzymatically rearrange to N^6-variants[12], which occurs in vivo during infection in mice[11]. The instability of 1-linked purines might account for their rarity in nature, but they are stable in acid environments, as in the mechanism proposed here. SAR studies with synthetic analogs directly demonstrate that the 1-linkage, the unusual and defining chemical feature of 1-TbAd, controls its biological activity. Thus, the revised model is that, among the last two steps of the natural TbAd biosynthetic pathway, 1-TbAd is the active metabolite that controls lysosomal function. N^6-TbAd largely lacks this function, but might have use as a species-specific diagnostic marker of infection.

Phagolysosomal acidification is a key outcome of the interferon-γ-mediated interactions between macrophages and T cells. The role of acidification as an upstream controller of phagolysosome maturation and intracellular killing has been recognized for decades[4,15], as has evidence for *Mtb*'s manipulation of this pathway[2,3]. Acidification blockade by *Mtb* is currently considered an immunoevasion mechanism resulting from bacterial blockade of vATPase delivery to infected phagosomes[6]. Although the previously known mechanism limits proton pumping into infected compartments, it is proposed that antacid release is a complementary mechanism that acts within phagosomes to scavenge protons that do arrive.

Lysosomal acidification controls the final mechanisms of intercellular lipid and protein degradation that are common to autophagy pathways. Autophagic degradation is co-opted during *Mtb* infection to generate intracellular inclusions[29,34], and chloroquine is perhaps the most widely used autophagy inhibitor in experimental settings[29]. In the present study similar pK_a values, potency and biological function of 1-TbAd and chloroquine have been outlined, pointing to a candidate role for 1-TbAd in autophagy inhibition. These observations support future development of synthetic 1-TbAd and analogs as lysosome-disrupting drugs. Related to this, both chloroquine and *Mtb* acid blockade limit MHC-II peptide loading[29], so 1-TbAd now becomes a candidate to influence MHC-II-mediated human T cell response.

Selective expression of 1-TbAd by *Mtb*, but not less virulent species, provides a correlative basis for proposing that 1-TbAd could be an evolved virulence factor. The *Rv3377c–Rv3378c* pathway is known only in an obligate human pathogen that continually grows under host immune pressure. Escape from acid-mediated killing could plausibly outweigh the metabolic costs of 1-TbAd biosynthesis. This hypothesis is supported by experimental data: transposon deletion of either *Rv3377c* or *Rv3378c* diminishes *Mtb* survival in mouse macrophages[14], and knock-in of these two genes confers a growth advantage in *M. kansasii*. Thus, these biological studies are consistent with the conclusion that the pH neutralization mechanism identified in the present study controls some aspect of *Mtb* growth and survival. The overarching questions going forward will be the extent to which this acid neutralization mechanism controls *Mtb* outcomes during natural infection in vivo, and whether it acts in the distinct phases of acute infection, persistence or transmission.

Online content

Any methods, additional references, Nature Research reporting summaries, source data, statements of code and data availability and associated accession codes are available at https://doi.org/10.1038/s41589-019-0336-0.

Received: 10 December 2018; Accepted: 28 June 2019;
Published online: 19 August 2019

References

1. *Global Tuberculosis Report* (WHO, 2018).
2. Armstrong, J. A. & Hart, P. D. Response of cultured macrophages to *Mycobacterium tuberculosis*, with observations on fusion of lysosomes with phagosomes. *J. Exp. Med.* **134**, 713–740 (1971).
3. Sturgill-Koszycki, S. et al. Lack of acidification in *Mycobacterium* phagosomes produced by exclusion of the vesicular proton-ATPase. *Science* **263**, 678–681 (1994).
4. Vandal, O. H., Nathan, C. F. & Ehrt, S. Acid resistance in *Mycobacterium tuberculosis*. *J. Bacteriol.* 191, 4714–4721 (2009).

5. McKinney, J. D. et al. Persistence of *Mycobacterium tuberculosis* in macrophages and mice requires the glyoxylate shunt enzyme isocitrate lyase. *Nature* **406**, 735–738 (2000).
6. Russell, D. G. Phagosomes, fatty acids and tuberculosis. *Nat. Cell Biol.* **5**, 776–778 (2003).
7. Behr, M. A. et al. Comparative genomics of BCG vaccines by whole-genome DNA microarray. *Science* **284**, 1520–1523 (1999).
8. Layre, E. et al. A comparative lipidomics platform for chemotaxonomic analysis of *Mycobacterium tuberculosis*. *Chem. Biol.* **18**, 1537–1549 (2011).
9. Galagan, J. E. et al. The *Mycobacterium tuberculosis* regulatory network and hypoxia. *Nature* **499**, 178–183 (2013).
10. Layre, E. et al. Molecular profiling of *Mycobacterium tuberculosis* identifies tuberculosinyl nucleoside products of the virulence-associated enzyme Rv3378c. *Proc. Natl Acad. Sci. USA* **111**, 2978–2983 (2014).
11. Pan, S. J. et al. Biomarkers for tuberculosis based on secreted, species-specific, bacterial small molecules. *J. Infect. Dis.* **212**, 1827–1834 (2015).
12. Young, D. C. et al. In vivo biosynthesis of terpene nucleosides provides unique chemical markers of *Mycobacterium tuberculosis* infection. *Chem. Biol.* **22**, 516–526 (2015).
13. Layre, E., de Jong, A. & Moody, D. B. Human T cells use CD1 and MR1 to recognize lipids and small molecules. *Curr. Opin. Chem. Biol.* **23c**, 31–38 (2014).
14. Pethe, K. et al. Isolation of *Mycobacterium tuberculosis* mutants defective in the arrest of phagosome maturation. *Proc. Natl Acad. Sci. USA* **101**, 13642–13647 (2004).
15. Vandal, O. H., Pierini, L. M., Schnappinger, D., Nathan, C. F. & Ehrt, S. A membrane protein preserves intrabacterial pH in intraphagosomal *Mycobacterium tuberculosis*. *Nat. Med.* 14, (849–854 (2008).
16. Heyl, A., Riefler, M., Romanov, G. A. & Schmulling, T. Properties, functions and evolution of cytokinin receptors. *Eur. J. Cell Biol.* **91**, 246–256 (2012).
17. Cekic, C. & Linden, J. Purinergic regulation of the immune system. *Nat. Rev.* **16**, 177–192 (2016).
18. MacMicking, J. D. Cell-autonomous effector mechanisms against *Mycobacterium tuberculosis*. *Cold Spring Harb. Perspect. Med.* **4**, a018507 (2014).
19. Rohde, K., Yates, R. M., Purdy, G. E. & Russell, D. G. *Mycobacterium tuberculosis* and the environment within the phagosome. *Immunol. Rev.* **219**, 37–54 (2007).
20. Deretic, V. et al. Immunologic manifestations of autophagy. *J. Clin. Invest.* **125**, 75–84 (2015).
21. Kapinos, L. E., Operschall, B. P., Larsen, E. & Sigel, H. Understanding the acid–base properties of adenosine: the intrinsic basicities of N1, N3 and N7. *Chemistry* **17**, 8156–8164 (2011).
22. Martin, M. G. & Reese, C. B. Some aspects of the chemistry of *N*(1)- and *N*(6)-dimethylallyl derivatives of adenosine and adenine. *J. Chem. Soc. Perkin* **1**, 1731–1738 (1968).
23. Winterbourn, C. C., Hampton, M. B., Livesey, J. H. & Kettle, A. J. Modeling the reactions of superoxide and myeloperoxidase in the neutrophil phagosome: implications for microbial killing. *J. Biol. Chem.* **281**, 39860–39869 (2006).
24. Buter, J. et al. Stereoselective synthesis of 1-tuberculosinyl sdenosine: a virulence factor of *Mycobacterium tuberculosis*. *J. Org. Chem.* **81**, 6686–6696 (2016).
25. Tan, S., Yates, R. M. & Russell, D. G. *Mycobacterium tuberculosis*: readouts of bacterial fitness and the environment within the phagosome. *Methods Mol. Biol.***1519**, 333–347 (2017).
26. Podinovskaia, M., Lee, W., Caldwell, S. & Russell, D. G. Infection of macrophages with *Mycobacterium tuberculosis* induces global modifications to phagosomal function. *Cell Microbiol.* **15**, 843–859 (2013).
27. de Duve, C. et al. Commentary. Lysosomotropic agents. *Biochem. Pharmacol.* **23**, 2495–2531 (1974).
28. Nadanaciva, S. et al. A high content screening assay for identifying lysosomotropic compounds. *Toxicology In Vitro* **25**, 715–723 (2011).
29. Plantone, D. & Koudriavtseva, T. Current and future use of chloroquine and hydroxychloroquine in infectious, immune, neoplastic, and neurological diseases: a mini-review. *Clin. Drug Invest.* **38**, 653–671 (2018).
30. Feng, X. et al. Antiinfectives targeting enzymes and the proton motive force. *Proc. Natl Acad. Sci. USA* **112**, E7073–E7082 (2015).
31. Mann, F. M. et al. Edaxadiene: a new bioactive diterpene from *Mycobacterium tuberculosis*. *J. Am. Chem.Soc.* **131**, 17526–17527 (2009).
32. Sani, M. et al. Direct visualization by cryo-EM of the mycobacterial capsular layer: a labile structure containing ESX-1-secreted proteins. *PLoS Pathog.* **6**, e1000794 (2010).
33. Samanovic, M. I. et al. Proteasomal control of cytokinin synthesis protects *Mycobacterium tuberculosis* against nitric oxide. *Mol. Cell* **57**, 984–994 (2015).
34. Deretic, V. Autophagy in tuberculosis. *Cold Spring Harb. Perspect. Med.* **4**, a018481 (2014).

Acknowledgements

The authors thank H. van Veen and W. Tigchelaar for EM, P. Reinink for phylogenetic graphs and S. Suliman for advice. Work was supported by grant nos. AI116604 (to D.B.M. and N.N.v.d.W.), AI111224 (to D.B.M. and M.M.), GM065307 (to E.O.), CA158191 (to E.O.) and AI114952 (to S.T.), the Dutch Science Foundation NWO-VICI 70.57.443 (to A.J.M.) and a Canadian Institute of Health Research Foundation grant 148362 (to M.A.B.).

Author contributions

H.B., R.C. and M.M. carried out the patient studies. T.Y.C. carried out the confocal microscopy. T.Y.C. and T.E. carried out the flow cytometry. M.A.B., M.G., J.W., M.B.R. and D.C.Y. carried out the *M. kansasii* assays. S.R., A.K.R. and E.L. performed the lipid analysis. J.A.M. performed the statistical analysis. J.B., A.R.P., A.M. and B.B.S. performed the chemical synthesis. E.O. and X.F. did the IMV studies. N.N.v.d.W. and A.E.G. performed the EM. S.R. carried out the gene deletion. S.R., N.S. and S.W. carried out the infection studies. S.T.carried out the pH measurements. The experiments were designed by D.B.M., E.J.R., M.A.B., E.O., N.N.v.d.W., S.E., A.J.M., T.Y.C., S.T. and J.B. The manuscript was written by D.B.M., J.B. and A.J.M., with contributions from all authors.

Competing interests

The authors declare no competing interests.

Additional information

Supplementary information is available for this paper at https://doi.org/10.1038/s41589-019-0336-0.

Correspondence and requests for materials should be addressed to D.B.M.

Methods

Patient-derived *Mtb* strains. *Mtb* strains were cultivated from the sputum of human TB patients recruited in or near Lima Peru by Socios en Salud under oversight from the Institutional Committee of Ethics in Research of the Peruvian Institutes of Health, the Institutional Review Board of the Harvard Faculty of Medicine and the Partners Healthcare IRB. Peruvian patients provided oral and written informed consent in Spanish.

Flow cytometry of human myeloid cells. Monocyte-derived dendritic cells were prepared by plating human monocytes in a 24-well plate (1×10^6) with 30 ng ml^{-1} of granulocyte–macrophage colony-stimulating factor (GM-CSF) (Peprotech 300-03) and 40 ng m^{-1} of interleukin-4 (200-04; Peprotech) for 3 d. The cells were then treated with synthetic 1-TbAd, natural 1-TbAd, Pam3Cys-SKKKK (L2000, EMC Microcollections) or medium for another day. Cells were then washed and collected for FACS analysis. For cell-surface protein detection, cells were stained with mouse anti-human CD1a (OKT6; in-house purified), CD80 (557223), CD86 (555655), CD14 (550376; BD Pharmingen), and isotype controls for immunoglobulin G (IgG)1 (P3; in-house purified) or IgG2a (14-4724-B1, eBioscience) followed by a fluorescein isothiocyanate-conjugated, goat anti-mouse IgG F(ab′)2 (A-10683, Thermo Fisher Scientific), then measured by a FACS Canto Flow Cytometer (BD) and analyzed using FlowJo.

Acidification and phagocytosis. THP-1 cells were obtained from the American Type Culture Collection (ATCC) and cultured in RPMI 1640 medium supplemented with 10% fetal bovine serum (FBS), L-glutamine, penicillin–streptomycin, 2-mercaptoethanol and 10 mM 4-(2-hydroxyethyl)-1-piperazine-ethanesulfonic acid (Hepes). Green fluorescent beads (silica, 3 µM, excitation/emission: 485/510 nm, Kisker Biotech). The beads were washed five times with phosphate-buffered saline (PBS) and stored in 0.5% bovine serum albumin (BSA) in PBS (10^8 beads ml^{-1}) at 4 °C. Beads were then resuspended in complete media plus 10% human serum (Gemini) for 10 min before the phagocytosis assay. To generate macrophage-like cells, THP-1 cells were plated on cover slips in 24-well plates (3×10^5) and treated with phorbol 12-myristate 13-acetate (p1585; Sigma-Aldrich), 50 nM, for 72 h. The differentiated cells were washed twice, then rested in fresh media for 4 h, followed by lipid treatment for 2 h. Lipid samples were vortexed and sonicated for 2 min before being added to the cells. Cells were then fed with excess fluorescent beads (4 beads per cell) and centrifuged at 1,000*g* for 1 min before incubation at 37 °C. After 30 min, cells were washed with PBS three times to remove extracellular beads, then treated with 250 nM LysoTracker-red DND-99 (L7528, Thermo Fisher Scientific) at 37 °C for 60 min. To assess washing and surface adherence, pilot studies showed that beads were rarely found outside the margin of cells (<2%) and more than 80% of beads penetrated to LAMP-1$^+$ compartments. Cells were washed, then fixed with 4% paraformaldehyde at room temperature for 20 min before the cover slips were mounted on the slides. Slides were analyzed on a Nikon Eclipse TE2000-UC1 confocal microscope by counting 5 low power fields (~200 cells).

Measurement of pH in mouse macrophages. To generate carboxyfluorescein beads for analysis of phagosomal pH, 50 µg carboxyfluorescein succinimidyl ester (Invitrogen) was added to 12.5 mg carboxylated, 3-µm silica beads (Kisker Biotech) that had been covalently linked to human IgG (Sigma-Aldrich) and defatted BSA[26]. After incubation on a nutator for 90 min at room temperature, the carboxyfluorescein beads were washed and stored in PBS at 4 °C. Bone marrow-derived macrophages were isolated from C57BL/6J mice (Jackson Laboratories), and maintained in Dulbecco's modified Eagle's medium containing 10% FBS (Gibco), 15% L-cell-conditioned media, 2 mM L-glutamine (Sigma-Aldrich), 1 mM sodium pyruvate (Gibco) and antibiotics (penicillin–streptomycin) (Gibco), at 37 °C in a 5% CO_2 atmosphere. Macrophages, 2×10^5 per well, were seeded into 96-well, clear-bottom, black plates for assays (Corning Costar). Assays were performed 1–2 d after seeding in the 96-well plates. Macrophages were washed three times with assay buffer (PBS, pH 7.2, 5% FBS, 5 mM dextrose, 1 mM $CaCl_2$, 2.7 mM KCl, 0.5 mM $MgCl_2$), and assay buffer containing indicated concentrations of compounds, the identities of which were blinded to the technician, added back to each well as appropriate. Carboxyfluorescein beads at about two to five beads per macrophage in assay buffer containing compounds were then added, and bottom reads at 450/520 nm and 490/520 nm acquired every 2 min for 2 h on a Biotek Synergy H1 microplate reader. A total of five to six replicate wells per condition were used, with temperature maintained at 37 °C. The ratio of the carboxyfluorescein fluorescence signal at excitation 490 nm (pH sensitive) versus 450 nm (pH insensitive) provides a readout of relative pH[26]. Animal procedures adhered to the National Institutes of Health's *Guide for the Care and Use of Laboratory Animals*, with animal protocol (no. B2016-37) approval by the Institutional Animal Care and Use Committee at Tufts University, in accordance with the Association for Assessment and Accreditation of Laboratory Animal Care, US Department of Agriculture, and US Public Health Service guidelines.

Electron microscopy. For EM studies, human monocytes (5×10^6) were treated with M-CSF (25 ng ml^{-1}) and GM-CSF (2.5 ng ml^{-1}) for 6 d and treated with lipids or infected with *Mtb*. The infected cells were incubated 4 h and washed to remove extracellular bacteria. The cells were incubated for 4 d and fixed with 2% formaldehyde and 0.2% glutaraldehyde in 0.4 M PHEM buffer (240 mM 1,4-piperazinediethanesulfonic acid (Pipes), 100 mM Hepes, 40 mM ethylene glycol-bis(β-aminoethyl ether)-*N*,*N*,*N*′,*N*′-tetraacetic acid (EGTA), 8 mM $MgCl_2$). For the lipid treatment experiments, the cells were treated for 2 h with 20 µM lipid and the fixed cells were processed for EM as published[35]. For infection experiments, infected cells were incubated 4 h and washed to remove extracellular bacteria. The cells were incubated for 4 d and fixed with 2% formaldehyde and 0.2% glutaraldehyde in 0.4 M PHEM buffer (240 mM Pipes, 100 mM Hepes, 40 mM EGTA, 8 mM $MgCl_2$ (ref. [35]). For EM, samples were embedded in gelatin blocks and plunge frozen in liquid nitrogen, and 60-nm ultrathin sections were produced at −120 °C. Then immunogold labeling was performed using antibodies against CD63 (Sanquin), CD107A (Biolegend), EEA1 (Thermo Fisher Scientific), rabbit anti-mouse bridging antibody and 10-nm gold particles conjugated to protein A (Utrecht University). Sections were stained with uranyl acetate and analyzed in a blinded manner using TEM (FEI Tecnai G2 Spirit Biotwin) at 100 kV.

Genomic analysis and statistics. To discover possible orthologs, sequences of *Rv3377c* or *Rv3378c* from the National Center for Biotechnology Information *Mtb* H37Rv reference genome (NC_000962.3) were used to interrogate whole-genome sequences with the basic local alignment search tool (blastn) set at these parameters: base match score of 2, base mismatch score of −3, *E*-value threshold of 10, minimum word size of 11, gap penalty of 5 and gap extension penalty of 2.

Liposome assays. Phosphatidylcholine (Sigma-Aldrich P5394, 1.8 µmol) and cholesterol (C8667; Sigma-Aldrich, 0.73 µmol) were mixed in chloroform in a 50-ml glass tube. The solvent was evaporated under nitrogen to yield a thin film, which was then hydrated in citrate buffer (500 µl) with the desired pH (5.0 or 7.4) by vortexing, followed by six freeze–thaw cycles. Vesicle size was homogenized using a liposome extruder (Avanti Polar Lipids) through polycarbonate membranes (0.2 µm and 0.1 µm). Liposomes were dialyzed against PBS (pH 7.4, 1 l) overnight using a Slide-A-Lyzer MINI Dialysis Device with a 10-kDa cutoff value (100-µl device, Thermo Fisher Scientific). After dialysis, two batches of liposomes were adjusted to equal concentration (absorbance = 0.25 at 600 nm). The final liposomes were examined by TecnaiG2 Spirit BioTWIN EM at the Harvard Medical School Core EM Facility. Liposomes (25 µl) and chloroquine (Sigma-Aldrich, C662825, 50 µM PBS solution) were mixed in a small glass insert, placed in an Eppendorf tube and incubated in a Thermomixer at 37 °C. After 2 h, the mixtures were loaded on to a MicroSpin G-50 column (GE Healthcare) and eluted with PBS, and nine 100-µl fractions were collected. The amount of liposomes in each fraction was determined by optical density. The liposomes were dispersed with 3 µl of Triton X-100 (10%) and the amount of chloroquine in each fraction was measured by the absorption at 342 nm. For adenosine (Sigma-Aldrich, A9251) uptake, 25 µl of a PBS solution was mixed with 25 µl of liposomes, as described above except the final quantification steps. The collected fractions (100 µl each) were mixed with 0.5 ml of chloroform/methanol (1/2, v/v), vortexed and dried under nitrogen. Each dried fraction was re-dissolved in a mobile phase of hexane/isopropyl alcohol (70/30, v/v) and loaded to a 1200 series HPLC system using a normal phase column (Varian MonoChrom Diol: 3 µm × 150 × 2 mm^2) and analyzed using an Agilent 6520 Accurate Mass Q-TOF mass spectrometer, based on published methods[8]. Phosphatidylcholine (*m*/*z* 760.58, used as a surrogate for liposome content) and adenosine (*m*/*z* 268.10) were quantified by comparing the peak area of extracted-ion chromatograms with external standards. For 1-TbAd and N^6-TbAd uptake, the experiment was performed in triplicate. Of lipid sonicate (25 µl), 1 µg was mixed with 25 µl of liposomes and incubated at 37 °C. After 2 h, the mixtures were loaded on to a MicroSpin G-50 column. Due to lipid adherence to the liposomes, the eluate consisted of two fractions: a liposome-associated lipid fraction (lipids co-elute with liposomes) and a liposome-free lipid fraction (lipids that stay on the column). The PBS eluate (500 µl) and column contents (Sephadex G-50) were treated with chloroform/methanol (1/2) 2 ml and 0.5 ml, respectively. The PBS eluate and the column extracts were analyzed by liquid chromatography (LC)–MS–quadruple time of flight (QToF) as described above. Both 1-TbAd and N^6-TbAd were detected as *m*/*z* 540.35, at retention times of 23 and 5 min, respectively.

IMV assays. Synthetic TbAd-like compounds were tested in triplicate in a blinded fashion in four types of IMV assays using succinate or ATP as energy substrates and *E. coli* or *M. smegmatis* membranes in two independent experiments as described previously[16].

Knock-in of genes to *M. kansasii*. *M. kansasii* ATCC 12478 was transformed with an integrative vector (pMV306) that either carried no insert (empty vector), or a 2.4-kilobase PCR fragment containing *Rv3377-8c* under the control of a constitutive *hsp60* promoter (*Rv3377–Rv3378c*). Cell-associated lipids were extracted and subjected to MS analyses[10]. To measure *M. kansasii* survival at different pH, organisms were maintained at mid-log phase (OD_{600} 0.2–0.5), passed through 22-G and 25-G needles, centrifuged at 450*g* for 5 min to remove clumps, and resuspended in 20 ml medium with altered pH (prepared using 2 M HCl) at a theoretical OD_{600} of 0.01. Cultures were grown for 16 d in biological triplicates. At each time point, a volume of 100 µl was taken in duplicate from each culture

to measure the OD_{600} on a 96-well, tissue-culture plate (Falcon) using the Infinite M200 Pro NanoQuant spectrophotometer (Tecan).

Deletion and complementation of *Rv3378c*. *Mtb* strain H37Rv was used for complete deletion of *Rv3378c* using recombineering gene-replacement strategy[36]. A targeting construct consisting of 500 basepair-flanking regions of *Rv3378c* and the loxP–hygromycin–LoxP cassette was synthesized and cloned into a pUC57 vector. The linear DNA substrate was amplified from the vector, and electrophoretically transformed into the *Mtb* H37Rv strain carrying the pNit–recET–SacB–kan plasmid and induced to express recombinase. Transformed bacteria were plated on to 7H10 agar plates containing 50 μg ml^{-1} of hygromycin for selection of recombinants. The recombinants were further selected for the absence of pNit–recET–SacB–kan plasmid by growing the colonies on 7H10 plates containing 5% sucrose and hygromycin (50 μg ml^{-1}) and subsequently testing the colonies for absence of growth on 7H10 plates with kanamycin (25 μg ml^{-1}). The recombinant colonies were screened by PCR for target gene deletion and replacement by the hygromycin cassette. The PCR screening was performed using primers that amplify the 5′-junction, 3′-junction. The entire target gene locus is positive for the PCR product, indicating target gene replacement and negative for the target gene. Complementation was performed by integrating a single copy of the gene under the control of the MOP promoter in the pJEB402 vector[37].

Reporting Summary. Further information on research design is available in the Nature Research Reporting Summary linked to this article.

Data availability

Institutional review boards require confidentiality of patient data and biological material. Distribution of *Mtb* strains is subject to biosafety approvals. Otherwise, all data and reagents are available.

References

35. van der Wel, N. et al. *M. tuberculosis* and *M. leprae* translocate from the phagolysosome to the cytosol in myeloid cells. *Cell* **129**, 1287–1298 (2007).
36. Murphy, K. C., Papavinasasundaram, K. & Sassetti, C. M. Mycobacterial recombineering. *Methods Mol. Biol.* **1285**, 177–199 (2015).
37. Guinn, K. M. et al. Individual RD1-region genes are required for export of ESAT-6/CFP-10 and for virulence of *Mycobacterium tuberculosis*. *Mol. Microbiol.* **51**, 359–370 (2004).

nature research

Corresponding author(s): D. Branch Moody

Last updated by author(s): 2019/01/03

Reporting Summary

Nature Research wishes to improve the reproducibility of the work that we publish. This form provides structure for consistency and transparency in reporting. For further information on Nature Research policies, see Authors & Referees and the Editorial Policy Checklist.

Statistics

For all statistical analyses, confirm that the following items are present in the figure legend, table legend, main text, or Methods section.

n/a	Confirmed	
☐	☒	The exact sample size (*n*) for each experimental group/condition, given as a discrete number and unit of measurement
☐	☒	A statement on whether measurements were taken from distinct samples or whether the same sample was measured repeatedly
☐	☒	The statistical test(s) used AND whether they are one- or two-sided *Only common tests should be described solely by name; describe more complex techniques in the Methods section.*
☒	☐	A description of all covariates tested
☐	☒	A description of any assumptions or corrections, such as tests of normality and adjustment for multiple comparisons
☐	☒	A full description of the statistical parameters including central tendency (e.g. means) or other basic estimates (e.g. regression coefficient) AND variation (e.g. standard deviation) or associated estimates of uncertainty (e.g. confidence intervals)
☒	☐	For null hypothesis testing, the test statistic (e.g. *F*, *t*, *r*) with confidence intervals, effect sizes, degrees of freedom and *P* value noted *Give P values as exact values whenever suitable.*
☒	☐	For Bayesian analysis, information on the choice of priors and Markov chain Monte Carlo settings
☒	☐	For hierarchical and complex designs, identification of the appropriate level for tests and full reporting of outcomes
☒	☐	Estimates of effect sizes (e.g. Cohen's *d*, Pearson's *r*), indicating how they were calculated

Our web collection on statistics for biologists contains articles on many of the points above.

Software and code

Policy information about availability of computer code

Data collection	No software was used except for commercially available integrated software within the ELIspot reader, confocal microscope and mass spectrometer (Flowjo), which is described by name .
Data analysis	Some data analysis was accomplished using R and Prism, as described.

For manuscripts utilizing custom algorithms or software that are central to the research but not yet described in published literature, software must be made available to editors/reviewers. We strongly encourage code deposition in a community repository (e.g. GitHub). See the Nature Research guidelines for submitting code & software for further information.

Data

Policy information about availability of data

All manuscripts must include a data availability statement. This statement should provide the following information, where applicable:

- Accession codes, unique identifiers, or web links for publicly available datasets
- A list of figures that have associated raw data
- A description of any restrictions on data availability

The data that support the findings of this study are available from the corresponding author upon reasonable request. A data availability statement describing the usual IRB-based limits on data sharing was added and only BSL3 laboratories can obtainpathogenic mycobacteria.

Field-specific reporting

Please select the one below that is the best fit for your research. If you are not sure, read the appropriate sections before making your selection.

☒ Life sciences ☐ Behavioural & social sciences ☐ Ecological, evolutionary & environmental sciences

For a reference copy of the document with all sections, see nature.com/documents/nr-reporting-summary-flat.pdf

Life sciences study design

All studies must disclose on these points even when the disclosure is negative.

Sample size	The sample size was determined by using the minimal sample size (n = 3) needed for statistical analysis for standard deviation.
Data exclusions	No data was excluded from the analyses.
Replication	Reproducibility of the findings was confirmed by performing the experiments at least two times with the number of actual replicates described in each figure legend. Figures were made by showing all data or representative experiments, as described in each figure legend.
Randomization	No experimental groups were compared.
Blinding	For electron microscopy, ratiometric pH analyses and inverted membrane vesicle assays reagents were exchanged between laboratories in a blinded fashion.

Reporting for specific materials, systems and methods

We require information from authors about some types of materials, experimental systems and methods used in many studies. Here, indicate whether each material, system or method listed is relevant to your study. If you are not sure if a list item applies to your research, read the appropriate section before selecting a response.

Materials & experimental systems

n/a	Involved in the study
☐	☒ Antibodies
☐	☒ Eukaryotic cell lines
☒	☐ Palaeontology
☐	☒ Animals and other organisms
☐	☒ Human research participants
☒	☐ Clinical data

Methods

n/a	Involved in the study
☒	☐ ChIP-seq
☐	☒ Flow cytometry
☒	☐ MRI-based neuroimaging

Antibodies

Antibodies used	CD1a (OKT6; in-house purified); CD80 (#557223), CD86 (#555655), CD14 (#550376; BD Pharmingen), isotype controls for IgG1 (P3; in-house purified) or IgG2a (#14-4724-B1, eBioscience), FITC-conjugated goat anti-mouse IgG F(ab')2 (#A-10683, ThermoFisher Scientific), CD63 (#M1544, Sanquin), CD107A (#328607, Biolegend), EEA1 (#PA5-17228, Thermo Scientific), rabbit anti mouse bridging antibody and 10 nm gold particles conjugated to protein A (Utrecht University)
Validation	Anti-CD1a (OKT6) was purified in house and has been repeatedly validated on transfected cell lines over 20 years at the Brigham and Women's Hospital. Lysosomal markers and gold particles have been validated at Utrecht University against morphological criteria that include electron dense mulitlammalar appearance for anti-lysosomal antibodies. Macrophage surface markers (CD14, CD80, CD86) were validated by the manufacturer and revalidated at the Brigham and Women's hospital, which showed the expected patterns for staining on monocytes, immature DCs and mature DCs.

Eukaryotic cell lines

Policy information about cell lines

Cell line source(s)	THP-1 cells were purchased and banked.
Authentication	The cell lines used showed expected microscopic morphology and function of myeloid cells but were not otherwise authenticated.
Mycoplasma contamination	The cell lines were not tested for mycoplasma contamination due to the short nature of culture conditions.

Commonly misidentified lines (See ICLAC register)	none

Animals and other organisms

Policy information about studies involving animals; ARRIVE guidelines recommended for reporting animal research

Laboratory animals	The study involved ratiometric pH assays in mouse bone marrow macrophages that were carried out at Tufts University.
Wild animals	The study did not involve wild animals
Field-collected samples	Sputum was collected from tuberculosis patients in Peru (by Socios y Salud - Peru, as a part of the 'Tuberculosis Research Unit' consortium), previously banked and shared with our laboratory.
Ethics oversight	A statement of Ethcs and veterinary oversight at Tufts is provided in the manuscript.

Note that full information on the approval of the study protocol must also be provided in the manuscript.

Human research participants

Policy information about studies involving human research participants

Population characteristics	Sputum was collected from male and female HIV- tuberculosis patients in Peru above the age of 18.
Recruitment	Patients were either self referred to a health clinic or contacted after exposure to a known case. All patients were negative for HIV and proven to have tuberculosis based on sputum culture. There were no intergroup comparisons.
Ethics oversight	Human patients were recruited through Socios En Salud with practices approved through Partners in Health with a cross-referencing approval at the Brigham and Women's Hospital and Harvard as documented in the methods section of the manuscript.

Note that full information on the approval of the study protocol must also be provided in the manuscript.

Flow Cytometry

Plots

Confirm that:

☐ The axis labels state the marker and fluorochrome used (e.g. CD4-FITC).

☒ The axis scales are clearly visible. Include numbers along axes only for bottom left plot of group (a 'group' is an analysis of identical markers).

☒ All plots are contour plots with outliers or pseudocolor plots.

☐ A numerical value for number of cells or percentage (with statistics) is provided.

Methodology

Sample preparation	Human peripheral blood mononuclear cells were purified over a ficoll gradient.
Instrument	DB FACS Canto Flow Cytometer
Software	Flowjo version 10.
Cell population abundance	The only flow experiment uses total peripheral blood mononuclear cells that are relatively depleted of granulocytes by ficoll preparation and then subpopulations are identified according to surface staining with monoclonal antibodies. Please note that two of the boxes are purposefully unchecked due to the particular experimental design of Figure 1. We provide mean fluorescence values but do attempt to group cells so no percentage values are obtained. The flow experiment involves single color analysis only, so cross-detection is impossible and it would be very unusual to report the fluorophores in the figure in this situation. The fluorophores used are stated in the methods.
Gating strategy	We did not gate subsets of live cells so no gating strategy is shown to support Figure 1. (For studies of peripheral blood mononuclear cells routine quality control is done in all experiments, which selects for intermediate or high forward scatter and high live/dead stains.)

☒ Tick this box to confirm that a figure exemplifying the gating strategy is provided in the Supplementary Information.